

PCCP

Accepted Manuscript



This is an *Accepted Manuscript*, which has been through the Royal Society of Chemistry peer review process and has been accepted for publication.

Accepted Manuscripts are published online shortly after acceptance, before technical editing, formatting and proof reading. Using this free service, authors can make their results available to the community, in citable form, before we publish the edited article. We will replace this *Accepted Manuscript* with the edited and formatted *Advance Article* as soon as it is available.

You can find more information about *Accepted Manuscripts* in the [Information for Authors](#).

Please note that technical editing may introduce minor changes to the text and/or graphics, which may alter content. The journal's standard [Terms & Conditions](#) and the [Ethical guidelines](#) still apply. In no event shall the Royal Society of Chemistry be held responsible for any errors or omissions in this *Accepted Manuscript* or any consequences arising from the use of any information it contains.

Shallow-tunnelling correction factor for use with Wigner-Eyring transition-state theory

Yanchuan Zhang,^{*a} Judith B. Rommel,^a Marko T. Cvitaš,^b and Stuart C. Althorpe^a

Received Xth XXXX 20XX, Accepted Xth XXXXXXXXXX 20XX

First published on the web Xth XXXXXXXXXX 200X

DOI: 10.1039/b000000x

We obtain a shallow-tunnelling correction factor for use with Wigner-Eyring transition-state theory (TST). Our starting point is quantum transition state theory (QTST), which approximates the accurate quantum rate as the instantaneous flux through a delocalised transition-state ensemble of ring-polymers. Expanding the ring-polymer potential to second order gives the well-known Wigner tunnelling-factor which diverges at the cross-over temperature between deep and shallow tunnelling. Here, we show how to remove this divergence by integrating numerically over the two softest ring-polymer normal modes. This results in a modified Wigner correction factor involving a one-dimensional integral evaluated along a straight line on the potential energy surface. Comparisons with accurate quantum calculations indicate that the newly derived correction factor gives realistic estimates of quantum rate coefficients in the shallow-tunnelling regime.

1 Introduction

In the most commonly used form of transition state theory (TST),^{1,2} the potential energy surface is expanded to second order about the saddle point, where the reaction coordinate is taken to be the unstable normal mode. The TST rate is then evaluated using

$$k^\ddagger(T) = \frac{k_B T}{h} \frac{Q^\ddagger(T)}{Q_r(T)} e^{-V^\ddagger/k_B T} \quad (1)$$

where T is the temperature, k_B is the Boltzmann constant, V^\ddagger is the potential energy at the saddle point, and $Q_r(T)$ and $Q^\ddagger(T)$ are harmonic (quantum) partition functions for the reactants and the saddle point (and approximate rotational partition functions are included in $Q_r(T)$ and $Q^\ddagger(T)$ when necessary). We will refer to $k^\ddagger(T)$ as the Wigner-Eyring TST rate coefficient.

Evidently $k^\ddagger(T)$ is a crude approximation. By expanding to second order, one has neglected the curvature of the reaction coordinate³ and decoupled it from the ro-vibrational motions orthogonal to it, thus reducing the calculation to an effective one-dimensional rate problem. In addition, the effects of anharmonicity and rotation-vibration coupling on the partition functions are completely neglected. However, given the difficulty of evaluating accurate potential energy surfaces on reaction barriers, it often seems fruitless to attempt to go beyond

Eq. (1), since by far the greatest errors are present in V^\ddagger . Furthermore, if the reaction is direct and recrossing is unimportant, and if quantum tunnelling can be safely ignored, Eq. (1) often gives a reasonable estimate of the order of magnitude of the rate coefficient and its dependence on T . Wigner-Eyring TST has therefore played a key role in the history of physical chemistry and continues to be used extensively.^{4–6}

A variety of methods have been developed for extending Wigner-Eyring TST to include quantum tunnelling, and thus to approximate the exact quantum rate.⁷ Such methods can broadly be divided into shallow-^{1,2,4,8} and deep-tunnelling methods,^{5,9–31} depending on how the tunnelling affects the quantum Boltzmann distribution. In shallow tunnelling, the Boltzmann distribution is delocalised by fluctuations around a point on top of the reaction barrier; in deep tunnelling,^{*} the fluctuations take place around a delocalised ‘instanton’ path, which typically bypasses the barrier via ‘corner cutting’. Unless the barrier is rather flat,³² shallow tunnelling dominates at temperatures above a cross-over temperature¹⁴

$$T_c = \frac{\hbar\omega^\ddagger}{2\pi k_B}, \quad (2)$$

where ω^\ddagger is the imaginary frequency at the saddle point of the system. Below this temperature, deep tunnelling gradually plays a larger role. Deep tunnelling dominates in electron-transfer reactions,³³ and in some hydrogen-transfer reactions (e.g. gas-phase hydrogen-transfer reactions at very low temperatures³⁴); but vast numbers of reactions, including many

^a Department of Chemistry, University of Cambridge, Lensfield Road, Cambridge CB2 1EW, United Kingdom. Tel: +44 (0) 1223 336373; E-mail: sca10@cam.ac.uk

^b Ruđer Bošković Institute, Department of Physical Chemistry, Bijenička Cesta 54, 10000 Zagreb, Croatia.

* Alternative definitions of ‘deep tunnelling’ can be found in the literature. We use the definition given in the Introduction throughout this article.

enzyme-^{35–37} and surface-catalysed^{38–41} hydride- and proton-transfer reactions are dominated by shallow tunnelling.

In this article, we derive a correction factor with which one can multiply Eq. (1) in order to obtain a realistic approximation of the accurate exact quantum rate in the shallow-tunnelling regime. The earliest shallow-tunnelling correction factor to be developed is the well-known expression of Wigner¹

$$\kappa_{\text{W}}(\beta) = \frac{\beta\hbar\omega^\ddagger/2}{\sin(\beta\hbar\omega^\ddagger/2)}. \quad (3)$$

where $\beta = 1/k_{\text{B}}T$. Unfortunately, this expression is of little practical use, since it diverges at the cross-over temperature T_{c} , and this divergence builds up gradually such that $\kappa_{\text{W}}(\beta)$ can overestimate the rate by orders of magnitude as the temperature approaches T_{c} from above. As a result, Eq. (3) is sometimes approximated to second order to give^{14,42}

$$\kappa_{\text{sW}}(\beta) = 1 + \frac{1}{24}(\beta\hbar\omega^\ddagger)^2. \quad (4)$$

This second order Wigner tunnelling factor (s-Wigner) does not diverge at cross-over, but there is no rigorous justification for using it (since it is the first term in a divergent series), except that it connects smoothly to the classical rate at high temperatures.

The shallow-tunnelling correction factor that we obtain in this article is obtained by modifying the Wigner correction factor (Eq. (3)), such that it does not diverge at T_{c} , and gives realistic estimates of the rate at $T \geq T_{\text{c}}$ (and in fact also at temperatures slightly below T_{c}). To obtain this factor, we start from the recently derived quantum transition-state theory (QTST) of Refs. 43–45, where it was shown that the definition of classical TST (as the instantaneous reactive flux through a dividing surface) generalizes to quantum mechanics. The difference between QTST and classical TST is that the former uses a *delocalised* dividing surface, which is expressed as a constraint on the imaginary-time path-integrals or ‘ring-polymers’ that describe the quantum Boltzmann statistics.^{46,47} Remarkably, QTST is identical[†] to a method developed earlier based on heuristic arguments, called ‘ring-polymer molecular dynamics’ (RPMD) TST.^{15,29,30} Thus QTST validates the growing body of quantum rate calculations done using the RPMD approach.^{29,30,33,36,48,49} An important special case of RPMD-TST is ‘centroid-TST’,^{25–28} in which the dividing surface is taken to be the centre-of-mass (centroid) of the polymer beads. The centroid dividing surface works well in the shallow-tunnelling regime,¹⁵ and will thus be used to obtain the tunnelling correction factor presented here.

The key equations of QTST are summarised in Section 2, after which we derive the new correction factor by modifying the derivation from QTST of the Wigner correction factor

$\kappa_{\text{W}}(T)$ (Eq. (3)). Section 3 presents comparisons with the exact quantum rates for one- and three-dimensional models. Section 4 concludes the article.

2 Derivation

2.1 Summary of quantum transition-state theory

Quantum transition-state theory^{43–45} (QTST) approximates the exact quantum rate coefficient^{7,10} by the instantaneous flux through a path-integral dividing surface. As mentioned in the introduction, QTST is equivalent to ring-polymer molecular dynamics (RPMD) TST.^{29,30,48} More precisely,

$$k_{\text{QTST}}(\beta) = \lim_{N \rightarrow \infty} k_{\text{RPMD-TST}}^{[N]}(\beta). \quad (5)$$

where $k_{\text{QTST}}(\beta)$ is the $t \rightarrow 0^+$ limit of the quantum flux-side time-correlation function introduced in Ref. 43, and $k_{\text{RPMD-TST}}^{[N]}(\beta)$ is the $t \rightarrow 0^+$ limit of the (classical) RPMD flux-side time-correlation function. The latter corresponds to applying classical rate theory in the extended (and fictitious) phase space occupied by the ring-polymer Hamiltonian. For a system with f degrees of freedom and classical Hamiltonian

$$H = \sum_{i=1}^f \frac{p_i^2}{2m_i} + V(x_1, \dots, x_f), \quad (6)$$

the ring-polymer Hamiltonian is^{46,50}

$$H_N(\mathbf{X}, \mathbf{P}) = \sum_{i=1}^f \sum_{j=1}^N \frac{P_{i,j}^2}{2m_i} + U_N(\beta_N, \mathbf{X}), \quad (7)$$

where $U_N(\beta_N, \mathbf{X})$ is

$$U_N(\beta_N, \mathbf{X}) = \sum_{j=1}^N V(X_{1,j}, \dots, X_{f,j}) + \sum_{i=1}^f \frac{m_i}{2(\beta_N \hbar)^2} \sum_{j=1}^N (X_{i,j+1} - X_{i,j})^2, \quad (8)$$

with $\beta_N = \beta/N$, and j defined cyclically such that $X_{i,N+1} = X_{i,1}$. In other words, the ring-polymer consists of N replicas of the original system, each located at $\mathbf{X}_j \equiv \{X_{1,j}, \dots, X_{f,j}\}$, which are joined into a loop by harmonic springs. Applying classical TST to this system, we obtain

$$k_{\text{RPMD-TST}}^{[N]}(\beta) Q_{\text{r}}(\beta) = \frac{1}{(2\pi\hbar)^{Nf}} \int d\mathbf{P} \int d\mathbf{X} e^{-\beta_N H_N(\mathbf{P}, \mathbf{X})} \times \delta[s(\mathbf{X})] v_{\text{s}}(\mathbf{P}, \mathbf{X}) h[v_{\text{s}}(\mathbf{P}, \mathbf{X})], \quad (9)$$

[†] We therefore use the terms QTST and RPMD-TST interchangeably.

where $Q_r(\beta)$ is the quantum partition function of the reactants (or equivalently the classical ring-polymer partition function of the reactants), and

$$v_s(\mathbf{P}, \mathbf{X}) = \sum_{i=1}^f \sum_{j=1}^N \frac{\partial s(\mathbf{X})}{\partial X_{i,j}} \frac{P_{i,j}}{m_i}. \quad (10)$$

is the flux through an $Nf - 1$ -dimensional dividing surface orthogonal to the reaction coordinate s .

Like classical TST, QTST assumes that there is no recrossing of the dividing surface,⁴⁵ and is therefore a good approximation for direct reactions. Unlike classical TST, QTST does not give a strict upper bound to the exact rate, because recrossing of quantum flux can sometimes increase the rate (by removing destructive interference). However, at temperatures sufficiently high that the amount of real-time coherence is small, QTST will give a *good approximation* to an upper bound to the exact rate, and one can thus proceed as in classical TST, by assuming that the optimal dividing surface is the one that minimises $k_{\text{QTST}}(\beta)$. If real-time coherence effects are large, then QTST is invalid and one has no choice but to attempt to compute the real-time quantum dynamics.

The reaction coordinate s must be invariant under cyclic permutation of the beads.⁴³ At temperatures $T > T_c$ (see Eq. (2)), the form of s that minimises recrossing is usually the centroid

$$s(\bar{\mathbf{x}}) = \frac{1}{N} \sum_{j=1}^N s_r(\mathbf{X}_j) \quad (11)$$

i.e. the centre-of-mass of the polymer beads along some (classical) reaction coordinate s_r . For asymmetric barriers at lower temperatures, s assumes a more general permutationally invariant form, which involves functions of the normal modes of the ring-polymer.¹⁵

2.2 Deriving the Wigner correction factor from QTST

To derive the Wigner correction factor $\kappa_{\text{W}}(T)$ from the QTST rate of Eq. (9), one approximates the integrals over \mathbf{X} by steepest-descent, meaning that the ring-polymer potential $U_N(\beta_N, \mathbf{X})$ is expanded to second order about its saddle point, such that the integrand becomes a product of Gaussian functions. This is a standard derivation, and we give here just the steps we will need (in Sec. 2.3) to derive a non-divergent modification to $\kappa_{\text{W}}(T)$. Mass-weighted coordinates are used for the rest of Sec. 2.

At $T > T_c$, the saddle point on $U_N(\beta_N, \mathbf{X})$ is located at the collapsed ring-polymer geometry

$$\mathbf{X}^\ddagger \equiv \{\mathbf{x}^\ddagger, \dots, \mathbf{x}^\ddagger\} \quad (12)$$

in which each replica is located at the saddle point \mathbf{x}^\ddagger on $V(\mathbf{x})$, so that

$$\beta_N U_N(\mathbf{X}^\ddagger) = \beta V(\mathbf{x}^\ddagger) \equiv \beta V^\ddagger \quad (13)$$

The second-order expansion of $U_N(\mathbf{X})$ about \mathbf{X}^\ddagger gives

$$U_N(\mathbf{Q}) \simeq U_N(\mathbf{Q}^\ddagger) + \frac{1}{2} \sum_{i=0}^{f-1} \sum_{j=0}^{N-1} \eta_{i,j}^2 (Q_{i,j} - Q_{i,j}^\ddagger)^2 \quad (14)$$

where $Q_{i,j}$ and $\eta_{i,j}$ ($i = 0, f-1, j = 0, N-1$) are the normal modes and frequencies given in the Appendix, and

$$\begin{aligned} Q_{i,j}^\ddagger &= \sqrt{N} x_i^\ddagger & \text{for } j = 0 \\ Q_{i,j}^\ddagger &= 0 & \text{otherwise} \end{aligned} \quad (15)$$

Each of the modes $Q_{i,j}$ describes a stretch of the ring-polymer along the direction of the i -th normal mode q_i on $V(\mathbf{x})$ at \mathbf{x}^\ddagger . The unstable mode on $U_N(\mathbf{X})$ is $Q_{0,0}$, and the reaction coordinate s is taken to be the centroid,

$$\begin{aligned} s &= \frac{1}{\sqrt{N}} (Q_{0,0} - Q_{0,0}^\ddagger) \\ &= \frac{1}{N} \sum_{j=1}^N q_{0,j} - x_j^\ddagger \end{aligned} \quad (16)$$

The unstable mode $Q_{0,0}$ is held fixed (by the δ -function in Eq. (9)); hence the second-order expansion about \mathbf{x}_0^\ddagger factorizes Eq. (9) into $Nf - 1$ Gaussian integrals over the stable modes $Q_{i,j}$.

For each $i > 0$, the set of N integrals over $Q_{i,j}$ gives the quantum partition function for a harmonic oscillator with frequency ω_i ; together, these integrals give $Q^\ddagger(T)$ of Eq. (1) (if one also includes the same approximate rotational partition function). The remaining $N - 1$ Gaussian integrals over the modes $Q_{0,j \neq 0}$ thus give the correction factor

$$\begin{aligned} \kappa_{\text{W}}(\beta) &= N \prod_{j=1}^{N-1} \left(\frac{1}{2\pi\beta_N \hbar^2} \right)^{1/2} \int_{-\infty}^{\infty} dQ_{0,j} e^{-\beta_N \eta_{0,j}^2 Q_{0,j}^2 / 2} \\ &= N \prod_{j=1}^{N-1} \frac{1}{\beta_N \hbar \eta_{0,j}} \end{aligned} \quad (17)$$

Using the expressions for $\eta_{i,j}$ given in the Appendix, taking the limit $N \rightarrow \infty$, and using the identity in the Appendix of Ref. 29, we then obtain the expression for $\kappa_{\text{W}}(\beta)$ in Eq. (3).

2.3 Numerical Wigner approximation

We now explain how to remove the divergence from $\kappa_{\text{W}}(\beta)$ at $T = T_c$, to obtain a modified ‘numerical Wigner’ correction

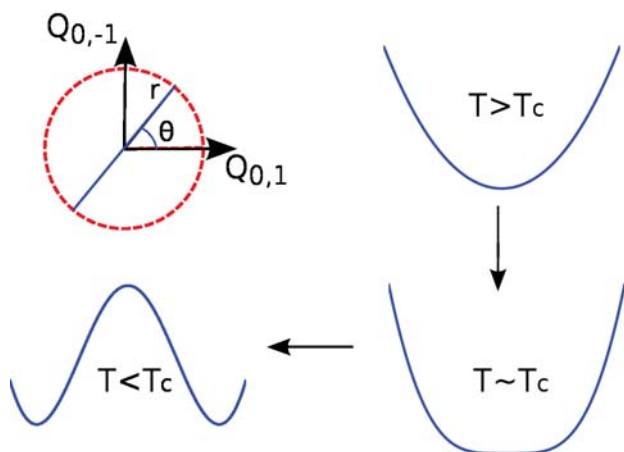


Fig. 1 Schematic plots of the part of the ring-polymer potential $\Delta U_N(Q_{0,1}, Q_{0,-1})$ that depends on the soft modes $Q_{0,\pm 1}$. Note that $\Delta U_N(Q_{0,1}, Q_{0,-1})$ is independent of the angle θ (shown top left), and that the plots show cuts through r (blue). The collapsed saddle point \mathbf{X}^\ddagger is at $r = 0$ in the $T > T_c$ plot; the instanton saddle point spreads around a circle which appears as a double-minimum in the cut through r at $T < T_c$.

factor (n-Wigner) $\kappa_{\text{nW}}(\beta)$ that is able to give a realistic estimate of the rate at temperatures down to (and in fact slightly below) $T = T_c$.

From Sec. 2.2, we see that $\kappa_{\text{W}}(\beta)$ allows for fluctuations in the Boltzmann distribution around the top of the barrier, in the direction of the unstable mode q_0 . These fluctuations are decoupled from the coordinates orthogonal to q_0 , which are treated harmonically as in Wigner-Eyring TST. This treatment is exact for a parabolic barrier, and correctly describes the infinite delocalisation in the Boltzmann distribution of such a system at $T = T_c$. The delocalisation is accounted for by the behaviour of the frequencies

$$\eta_{0,\pm 1} = \sqrt{\frac{4\pi^2}{(\beta\hbar)^2} - (\omega^\ddagger)^2} \quad (18)$$

which are real for $T > T_c$ and imaginary for $T < T_c$ (see Eq. (2)). Below T_c , the modes $Q_{0,\pm 1}$ (which control the overall extent of the Boltzmann distribution) can thus stretch indefinitely over the top of the barrier, which is what causes the integral to diverge.

In a real system,[‡] the rate does not diverge at $T = T_c$, but instead becomes dominated by deep tunnelling. On passing through T_c , the saddle point on $U_N(\mathbf{X})$ shifts to a geometry in which the polymer beads are distributed along the ‘instanton’, which is a periodic orbit on the upside-down potential

energy surface $-V(\mathbf{x})$.¹¹ One can still approximate Eq. (9) by steepest-descent in this regime, but now the calculation is more expensive, since one must expand about the instanton saddle point, which first needs to be located on the Nf -dimensional surface $U_N(\mathbf{X})$.^{15,17,31}

For $T > T_c$, on the other hand, the saddle point on $U_N(\mathbf{X})$ is the same for a real system as for a harmonic barrier, namely \mathbf{X}^\ddagger . However, the fluctuations around \mathbf{X}^\ddagger are different, since, in a real system, $Q_{0,\pm 1}$ samples increasingly anharmonic regions of $V(\mathbf{x})$ as T approaches T_c . This causes the steepest-descent approximation to break down. The neat distinction between deep and shallow tunnelling is thus an artefact of the steepest-descent approximation: for $T > T_c$, the tunnelling is predominantly ‘shallow’, since the polymer fluctuations take place around the collapsed saddle point \mathbf{X}^\ddagger , and most of the modes $Q_{i,j}$ make only small displacements away from it; but the soft modes $Q_{0,\pm 1}$ clearly sample regions of space that become increasingly distant from \mathbf{X}^\ddagger as T approaches T_c . At $T = T_c$, the dependence of $U_N(\mathbf{X})$ on $Q_{0,\pm 1}$ is completely flat near \mathbf{X}^\ddagger , as shown in Fig. 1.

We therefore propose relaxing the steepest-descent approximation in the modes $Q_{0,\pm 1}$, such that $U_N(\mathbf{X})$ is now approximated by

$$U_N(\mathbf{Q}) \simeq U_N(\mathbf{Q}^\ddagger) + \frac{1}{2} \sum_{i=0}^{f-1} \sum_{j=0}^{N-1} \eta_{i,j}^2 (Q_{i,j} - Q_{i,j}^\ddagger)^2 + \Delta U_N(Q_{0,1}, Q_{0,-1}) \quad (19)$$

where the prime indicates that the terms $i = 0, j = \pm 1$ are omitted from the sum, and $\Delta U_N(Q_{0,1}, Q_{0,-1})$ is the part of $U_N(\mathbf{X})$ that depends on $Q_{0,\pm 1}$ (when all the other $Q_{i,j}$ are set to $Q_{i,j}^\ddagger$). This approach is not perfect (since it neglects the coupling between $Q_{0,\pm 1}$ and the other modes, which is likely to become stronger as $Q_{0,\pm 1}$ becomes softer), but it is certainly an improvement on treating $Q_{0,\pm 1}$ by steepest-descent, since it is guaranteed not to diverge at $T = T_c$.

The dependence of $\Delta U_N(Q_{0,1}, Q_{0,-1})$ on $Q_{0,\pm 1}$ is illustrated schematically in Fig. 1. An important property of $\Delta U_N(Q_{0,1}, Q_{0,-1})$ is that it is independent of θ in the limit $N \rightarrow \infty$, where θ is the polar angle defined by

$$\begin{aligned} r &= \sqrt{Q_{0,1}^2 + Q_{0,-1}^2}, \\ \theta &= \arctan(Q_{0,-1}/Q_{0,1}). \end{aligned} \quad (20)$$

This symmetry follows from the invariance of $U_N(\mathbf{X})$ to cyclic permutation of the polymer beads (as may be easily demonstrated by writing $\Delta U_N(Q_{0,1}, Q_{0,-1})$ in terms of the bead coordinates \mathbf{X} , then changing $X_{i,j} \rightarrow X_{i,j+1}$). We may thus reduce the two-dimensional integral over $Q_{0,\pm 1}$ to a one-dimensional integral over r . On evaluating the integrals over the other modes by steepest descent (following Sec. 2.2), we

[‡] This analysis breaks down if the barrier-top is very flat. See Ref. 30

obtain

$$\kappa_{\text{nW}}(\beta) = \frac{N A_N(\beta)}{\beta_N \hbar^2} \int_0^\infty Q_{0,1} dQ_{0,1} e^{-\beta_N \Delta U_N(Q_{0,1}, 0)} \quad (21)$$

with

$$A_N(\beta) = \prod_{j=3}^{N-1} \frac{1}{\beta_N \hbar \eta_{0,j}} \quad (22)$$

This new shallow-tunnelling correction factor is the main result of the article, and will be referred to as the ‘numerical Wigner’ correction factor.

3 Numerical implementation

The computation of $\kappa_{\text{nW}}(\beta)$ has two parts: the evaluation of $A_N(\beta)$, and the numerical integration over $Q_{0,1}$. The evaluation of $A_N(\beta)$ demands little computational effort, since it requires only the frequencies ω_i at the saddle point of $V(\mathbf{x})$ (which will already have been obtained in the Wigner-Eyring calculation). Unlike $\kappa_{\text{W}}(\beta)$, $A_N(\beta)$ is not in closed form, which raises the question of how large to make N ; this parameter needs to be sufficiently large that $A_N(\beta)$ has converged with respect to N , but not so large that $A_N(\beta)$ becomes numerically difficult to evaluate. In practice, we expect that a value of N in the range of 100-300 will usually suffice (see below).

Having converged $A_N(\beta)$, one can then evaluate the integral over $Q_{0,1}$, which clearly will involve a non-trivial amount of computational effort, since $\Delta U_N(Q_{0,1}, 0)$ needs to be calculated along a set of points in $Q_{0,1}$. The most economical way to do this is to interpolate $V(\mathbf{x})$ along a grid of points on q_0 (centred on the saddle point), from which it is then straightforward to use Eq. (8) to generate $\Delta U_N(Q_{0,1}, 0)$ at all desired temperatures. To determine the maximum value of q_0 , it is best to generate $\Delta U_N(Q_{0,1}, 0)$ from $V(\mathbf{x})$ first at $T = T_c$, the temperature at which the polymers stretch furthest along $Q_{0,1}$, and to continue increasing $|Q_{0,1}|$ until $\exp[-\beta_N \Delta U_N(Q_{0,1}, 0)]$ becomes small; one then has an upper range sufficient for the integrals at all $T > T_c$. The integrand varies smoothly as a function of $Q_{0,1}$, and thus a large number of points is unlikely to be necessary.

Figure 2 plots the rate coefficients obtained from $\kappa_{\text{nW}}(\beta)$ for a set of one-dimensional models, and compares them with the coefficients obtained from $\kappa_{\text{W}}(\beta)$, and with the QTST, Wigner-Eyring TST and exact quantum results. The potentials used were Eckart barriers (E1-3) of the form

$$V(x) = \frac{V_1}{1 + \exp(-2x/a)} + \frac{[V_0^{1/2} + (V_0 - V_1)^{1/2}]^2}{4 \cosh^2(x/a)}, \quad (23)$$

with V_0 (barrier height) and V_1 (exothermicity) taking the values given in Table 1. More detailed comparisons (of the ratios

Table 1 Parameters (in atomic units) used to obtain the results in Fig. 2 and Table 2.

	a	m (mass)	V_0	V_1
E1	0.66047	1836	$72/(ma^2\pi^2)$	0
E2	0.66047	1836	0.009	-0.003
E3	$8/\sqrt{3\pi}$	1	$6/\pi$	$-18/\pi$

of the numerical Wigner to the exact quantum rate) are given in Table 2. For convergence $N = 128$ beads were used for E1 and $N = 256$ for E2 and E3. These results show that, as expected, the numerical Wigner rate does not diverge at $T = T_c$, and gives better results than the Wigner rate (Eq. (3)) for $T > T_c$. In fact, the numerical Wigner method continues to give a good estimate of the rate down to temperatures slightly below T_c . This ‘extra’ range of temperatures narrows as the barrier is made more asymmetric, which is to be expected, since increasing the asymmetry of the barrier is known to push the unstable mode away from the centroid more rapidly as temperature decreases.

Figure 3 and Table 3 show similar results for the (fully-dimensional) H + H₂, D + H₂ and H + CH₄ reactions, obtained using the potential energy surfaces of Refs. 51 & 52, where they are compared with accurate quantum and QTST results obtained previously^{31,53,54} using the same surfaces. The number of ring-polymer beads needed to converge the steepest-descent integrals was $N = 256$ for all cases. A total of 40 points distributed along q_0 were found to be sufficient to interpolate $V(\mathbf{x})$ and thus generate $\Delta U_N(Q_{0,1}, 0)$ for all $T > T_c$. The same overall improved agreement with the accurate quantum results is obtained as for the one-dimensional examples, but there is additional numerical error (Table 3) near cross-over (which gives rise to a fortuitous cancellation of errors in the case of H + CH₄). Most likely, this extra error is caused by the neglect of reaction-path curvature, since the soft modes $Q_{0,\pm 1}$ are likely to bend around the minimum energy path, mixing in other modes. Although these effects are unlikely to affect the order of magnitude of the predictions above cross-over (since the polymer stretches across a relatively small distance), they are nonetheless quite significant (Table 3). Further work may attempt to derive a correction for the neglect of curvature. A curious feature of these results is that the crude second-order approximation to $\kappa_{\text{W}}(\beta)$ (Eq. (4)) agrees closely with the numerical Wigner result (Fig. 3 and Table 3). Such close agreement is probably fortuitous (and was not found in the one-dimensional calculations—see Table 2).

As already mentioned, $\kappa_{\text{nW}}(\beta)$ continues to give reasonable estimates of the quantum rate coefficient over a range of

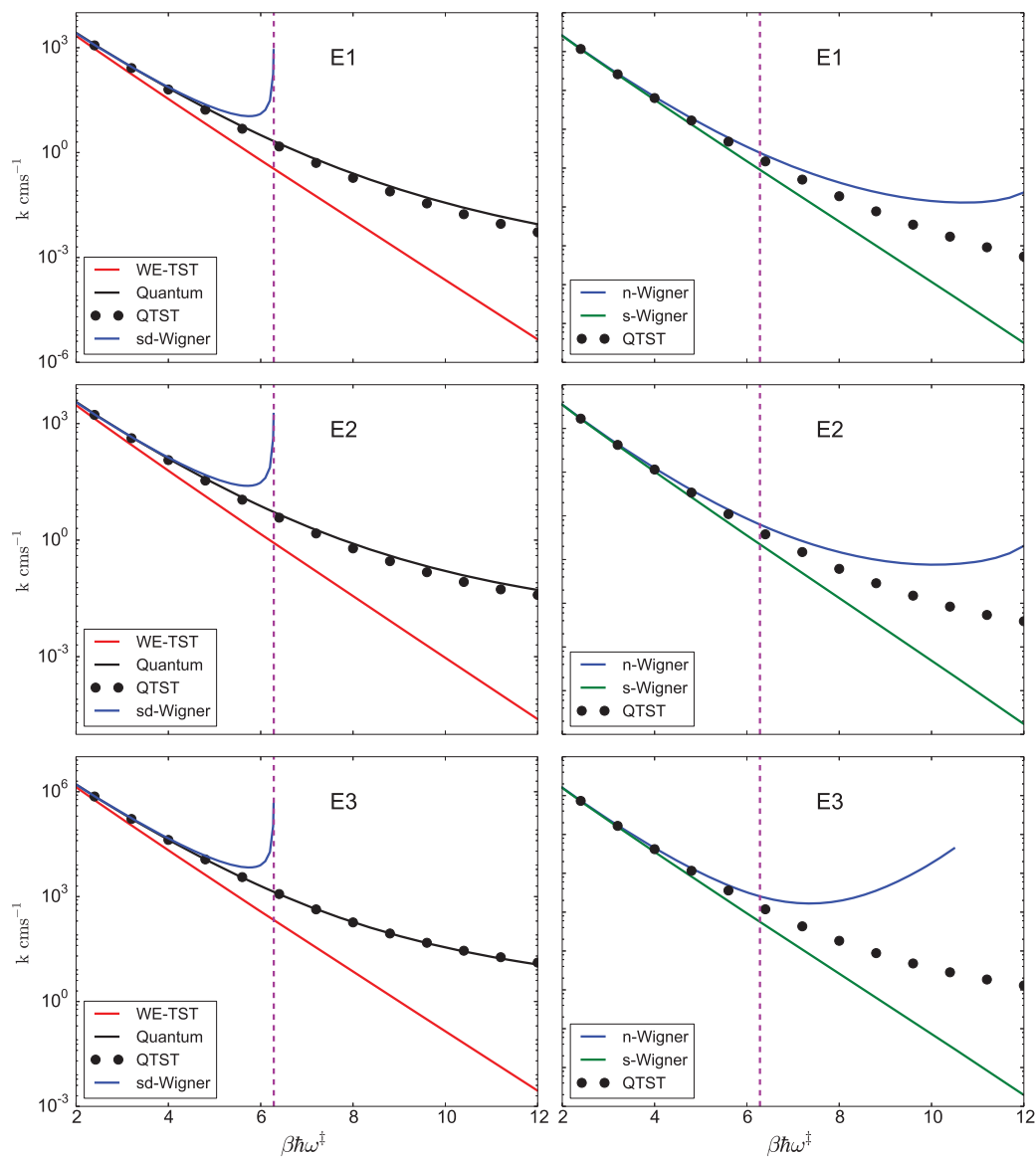


Fig. 2 Rate coefficients for the one-dimensional model systems E1-E3 of Table 1 showing that the newly developed numerical Wigner approach [n-Wigner: Eq. (21), right panels] gives a good approximation to QTST [Eq. (9)] at the cross-over temperature (dashed line), by removing the divergence from the standard Wigner approximation [sd-Wigner: Eq. (3), left panels]. Also shown are the results of Wigner-Eyring TST [WE-TST: Eq. (1)], the second-order truncated Wigner approximation [s-Wigner: Eq. (4)] and exact quantum calculations.

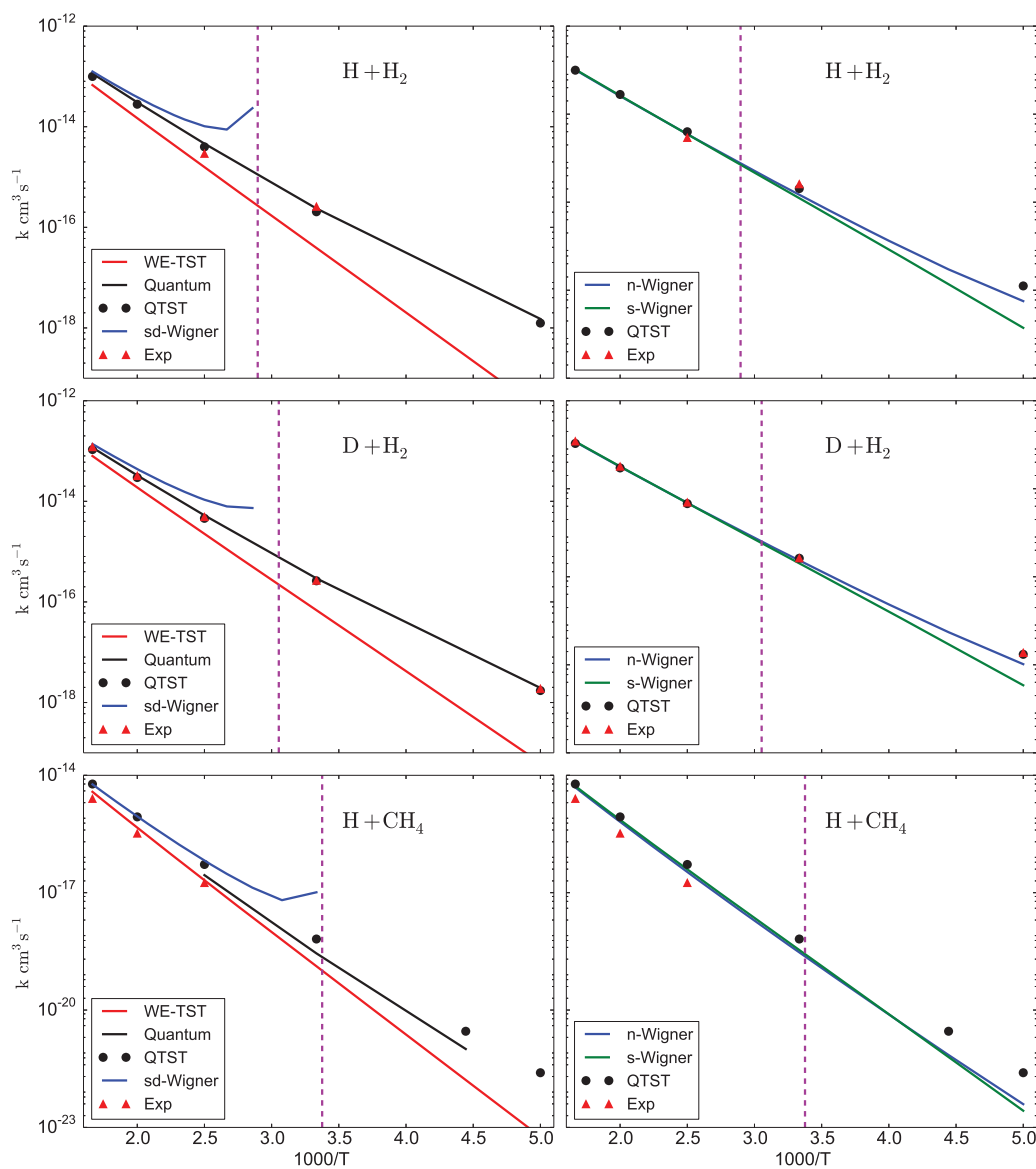


Fig. 3 Rate coefficients for the (fully-dimensional) $\text{H} + \text{H}_2$, $\text{D} + \text{H}_2$ and $\text{H} + \text{CH}_4$ reactions. The quantum calculations are taken from Refs. 31,53; the experimental results (Exp) from Refs. 54–56. All other abbreviations used are defined in Fig. 2.

Table 2 Ratios of approximate to exact quantum rate coefficients, computed for the one-dimensional model systems E1-E3 of Table 1. The abbreviations used are defined in Fig. 2.

$\beta\hbar\omega^\ddagger$	E1			E2			E3		
	QTST	n-Wigner	s-Wigner	QTST	n-Wigner	s-Wigner	QTST	n-Wigner	s-Wigner
2	0.96	0.97	0.95	0.96	0.97	0.96	0.97	0.98	0.96
4	0.91	0.98	0.81	0.91	0.98	0.81	0.93	0.99	0.80
6	0.84	1.12	0.48	0.85	1.15	0.48	0.88	1.15	0.44
8	0.75	1.69	0.17	0.76	1.82	0.16	0.85	1.94	0.12
10	0.66	3.89	0.03	0.74	4.77	0.03	0.84	5.58	0.01

Table 3 Ratios of approximate to accurate quantum rate coefficients,^{31,53} calculated for the H + H₂, D + H₂ and H + CH₄ reactions. The abbreviations used are defined in Fig. 2.

T (K)	H + H ₂			D + H ₂			T (K)	H + CH ₄		
	QTST	n-Wigner	s-Wigner	QTST	n-Wigner	s-Wigner		QTST	n-Wigner	s-Wigner
600	0.87	0.89	0.91	0.91	1.00	1.01				
500	0.92	0.84	0.86	0.91	0.96	0.98				
400	0.86	0.77	0.76	0.87	0.91	0.90	400	1.87	1.20	1.40
300	0.86	0.62	0.52	0.89	0.80	0.69	300	2.33	1.06	1.21
200	0.83	0.37	0.09	0.89	0.53	0.18	225	2.84	0.70	0.62

temperatures below T_c . This is because, at temperatures just below T_c , the instanton geometry depends mainly on $Q_{0,\pm 1}$ and is thus correctly included in the integral over r in Eq. (21). At such temperatures the potential $\Delta U_N(Q_{0,1}, Q_{0,-1})$ is flat, with the instanton geometry appearing as a shallow circular depression, *i.e.* a minimum along r . At lower temperatures, the instanton geometry mixes in modes other than $Q_{0,\pm 1}$, and appears as a pronounced minimum along r , giving rise to a corresponding maximum at $r=0$ (see Fig. 1). A reliable rule of thumb for determining whether the numerical Wigner rate is within 50% of the QTST rate is to observe whether the integrand in Eq. (21) has a noticeable slope at $r=0$; once the integrand becomes flat, then $\kappa_{nW}(\beta)$ can no longer be trusted to give a good estimate of the rate (see Fig. 4).

Finally, in pointing out the limitations of the numerical Wigner method, we should emphasize that, since it employs steepest-descent in all but two of the N_f modes, it is likely to break down if the potential energy surface $V(\mathbf{x})$ is strongly anharmonic near the barrier top, either in the direction of the reaction coordinate or perpendicular to it. Two examples bear this out. Figure 5a plots the rates obtained for the H + Cl₂ reaction, in which the barrier top is flat in the direction of the reaction coordinate. The concept of a cross-over temperature (which is based on a harmonic analysis) breaks down in this system, which supports instantons at $T > T_c$. Such behaviour may be quite common³² and is probably tractable by instanton

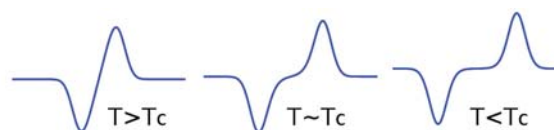


Fig. 4 Plots showing the shape of the integrand in Eq. (21) as a function of $Q_{0,1}$. The numerical Wigner method gives a reasonable approximation to the quantum rate until a maximum develops at $Q_{0,1} = 0$, such that the integrand becomes flat at the origin as shown in the rightmost plot. These plots were obtained for the one-dimensional E1 system; similar behaviour was found for all other systems tested.

methods. Figure 5b shows the results for Cl + HCl; the barrier is flat perpendicular to the reaction coordinate, and thus the numerical Wigner method fails (as also does the Wigner-Eyring method at classical temperatures).

4 Conclusions

We have proposed a simple correction factor for including the effects of shallow tunnelling into the Wigner-Eyring TST rate. This ‘numerical Wigner’ factor is similar to the well-known Wigner correction factor (Eq. (3)), except that the degenerate modes that cause the latter to diverge at the cross-over tem-

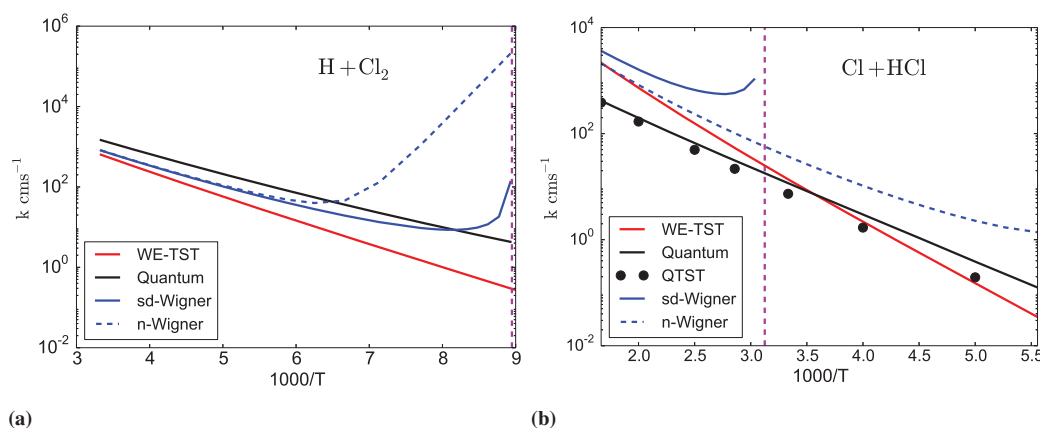


Fig. 5 Computational results for the collinear H + Cl₂ and Cl + HCl reactions, showing how the numerical Wigner approach breaks down if the potential is flat along the reaction coordinate (H + Cl₂) or perpendicular to it (Cl + HCl).

perature are integrated over numerically. The resulting correction factor does not diverge at the cross-over temperature, and gives realistic estimates of the quantum rate down to temperatures slightly below cross-over. The extra computational effort required (in addition to evaluating the Wigner-Eyring TST rate) is to evaluate a one-dimensional integral along a straight line in the direction of the unstable mode at the saddle point. Typically, the integral requires the potential energy to be calculated at about 30-40 points along this line. We thus expect the new correction factor to be computable for a large variety of systems, certainly for proton and hydride transfer in complex gas-phase systems,³⁷ and possibly also for proton and hydride-transfer reactions in solution (provided one is able to free-energy average over the solvent modes).

The disadvantage of the method is that it neglects the effects of reaction-path curvature on the tunnelling, although this was found to have a relatively minor effect in the numerical tests carried out here (most likely because the fluctuations in the QTST partition function do not extend far along the reaction coordinate at shallow-tunnelling temperatures). The advantages of the method are that it does not need additional optimisation calculations to be done (once the classical saddle-point is located), and that it is based, not on a heuristic model, but on a systematic approximation to the QTST rate.

Acknowledgements

We thank Timothy J. H. Hele for commenting on the manuscript. YZ acknowledges funding from the British Council in New Zealand and the University of Cambridge. JBR thanks the Humboldt foundation for a Feodor-Lynen research fellowship. SCA acknowledges funding from the Cambridge Newton Trust.

APPENDIX: Ring-polymer normal modes

Let the f mass-scaled normal modes of the potential energy surface $V(\mathbf{x})$ at the saddle point \mathbf{x}_0^\ddagger be $q_i, i = 0, \dots, f - 1$, with ω_i being the associated frequencies, and define q_0 to be the unstable normal mode (i.e. the reaction coordinate in Eq. (1)), so that $\omega_0 = i\omega^\ddagger$, where ω^\ddagger is the modulus of the barrier frequency.

The Nf normal modes of the ring-polymers at the collapsed ring-polymer saddle point \mathbf{x}^\ddagger are then

$$\begin{aligned} Q_{i,0} &= \frac{1}{\sqrt{N}} \sum_{j=1}^N q_{i,j}, \\ Q_{i,k} &= \sqrt{\frac{2}{N}} \sum_{j=1}^N \sin\left(\frac{2kj\pi}{N}\right) q_{i,j}, \\ Q_{i,N-k} \equiv Q_{i,-k} &= \sqrt{\frac{2}{N}} \sum_{j=1}^N \cos\left(\frac{2kj\pi}{N}\right) q_{i,j}, \\ Q_{i,N/2} &= \frac{1}{\sqrt{N}} \sum_{j=1}^N (-1)^j q_{i,j}. \end{aligned} \quad (24)$$

where $i = 0, \dots, f - 1$ and $k = 1, \dots, (N - 2)/2$. The associated frequencies are

$$\eta_{i,k} = \sqrt{\frac{4}{(\beta_N \hbar)^2} \sin^2\left(\frac{k\pi}{N}\right) + \omega_i^2}, \quad (25)$$

where $k = -(N - 2)/2, \dots, 0, \dots, (N - 2)/2, N/2$. Note that the modes $Q_{i,\pm k}$ are degenerate.

In the limit $N \rightarrow \infty$, only modes with $k \ll N$ have non-zero probability in the ring-polymer distribution, and their fre-

quencies become

$$\eta_{i,k} = \sqrt{\left(\frac{2k\pi}{\beta\hbar}\right)^2 + \omega_i^2}, \quad k \ll N. \quad (26)$$

References

- 1 E. Wigner, *Z. Phys. Chem. B*, 1932, **19**, 203–216.
- 2 H. Eyring, *J. Chem. Phys.*, 1935, **3**, 107.
- 3 W. H. Miller, N. C. Handy and J. E. Adams, *J. Chem. Phys.*, 1980, **72**, 99.
- 4 D. G. Truhlar, B. C. Garrett and S. J. Klippenstein, *J. Phys. Chem.*, 1996, **100**, 12771.
- 5 D.-H. Lu, T. N. Truong, V. S. Melissas, G. C. Lynch, Y.-P. Liu, B. C. Garrett, R. Steckler, A. D. Issacson, S. N. Rai, G. C. Hancock, J. G. Lauderdale and D. G. Truhlar, *Comput. Phys. Commun.*, 1992, **71**, 235–262.
- 6 E. Pollak and P. Talkner, *Chaos*, 2005, **15**, 026116.
- 7 W. H. Miller, S. D. Schwartz and J. W. Tromp, *J. Chem. Phys.*, 1983, **79**, 4889.
- 8 W. H. Miller, R. Hernandez, N. C. Handy, D. Jayatilaka and A. Willetts, *Chem. Phys. Lett.*, 1990, **172**, 62.
- 9 R. A. Marcus and M. E. Coltrin, *J. Chem. Phys.*, 1977, **67**, 2609.
- 10 W. H. Miller, *J. Chem. Phys.*, 1974, **61**, 1823.
- 11 W. H. Miller, *J. Chem. Phys.*, 1975, **62**, 1899–1906.
- 12 S. Chapman, B. C. Garrett and W. H. Miller, *J. Chem. Phys.*, 1975, **63**, 2710.
- 13 C. G. Callan and S. Coleman, *Phys. Rev. D*, 1977, **16**, 1762.
- 14 V. A. Benderskii, D. E. Makarov and C. A. Wight, *Adv. Chem. Phys.*, 1994, **88**, 55.
- 15 J. O. Richardson and S. C. Althorpe, *J. Chem. Phys.*, 2009, **131**, 214106.
- 16 S. C. Althorpe, *J. Chem. Phys.*, 2011, **134**, 114104.
- 17 J. B. Rommel, T. P. M. Goumans and J. Kästner, *J. Chem. Theory Comput.*, 2011, **7**, 690–698.
- 18 J. B. Rommel and J. Kästner, *J. Chem. Phys.*, 2011, **134**, 184107.
- 19 Y. Wang and J. M. Bowman, *J. Chem. Phys.*, 2008, **129**, 121103.
- 20 Y. Wang and J. M. Bowman, *J. Chem. Phys.*, 2013, **139**, 154303.
- 21 X. Sun, H. Wang and W. H. Miller, *J. Chem. Phys.*, 1998, **109**, 7064.
- 22 H. Wang, X. Sun and W. H. Miller, *J. Chem. Phys.*, 1998, **108**, 9726.
- 23 J. Liu and W. H. Miller, *J. Chem. Phys.*, 2007, **127**, 114506.
- 24 W. H. Miller, Y. Zhao, M. Ceotto and S. Yang, *J. Chem. Phys.*, 2003, **119**, 1329.
- 25 M. J. Gillan, *Phys. Rev. Lett.*, 1987, **58**, 563–566.
- 26 M. J. Gillan, *J. Phys. C*, 1987, **20**, 3621–3641.
- 27 J. Cao and G. A. Voth, *J. Chem. Phys.*, 1994, **100**, 5106–5117.
- 28 S. Jang and G. A. Voth, *J. Chem. Phys.*, 1999, **111**, 2371.
- 29 I. R. Craig and D. E. Manolopoulos, *J. Chem. Phys.*, 2005, **122**, 084106.
- 30 I. R. Craig and D. E. Manolopoulos, *J. Chem. Phys.*, 2005, **123**, 034102.
- 31 S. Andersson, G. Nyman, A. Arnaldsson, U. Manthe and H. Jónsson, *J. Phys. Chem. A*, 2009, **113**, 4468–4478.
- 32 S. Alvarez-Barcia, J. R. Flores and J. Kästner, *J. Phys. Chem. A*, 2014, **118**, 78–82.
- 33 A. R. Menzeleev, N. Ananth and T. F. Miller III, *J. Chem. Phys.*, 2011, **135**, 074106.
- 34 R. J. Shannon, M. A. Blitz, A. Goddard and D. E. Heard, *Nat. Chem.*, 2013, **5**, 745–9.
- 35 L. Masgrau, K. E. Ranaghan, N. S. Scrutton, A. J. Mulholland and M. J. Sutcliffe, *J. Phys. Chem. B*, 2007, **111**, 3032.
- 36 N. Boekelheide, R. Salomón-Ferrer and T. F. Miller III, *Proc. Natl. Acad. Sci. U. S. A.*, 2011, **108**, 16159–63.
- 37 J. B. Rommel, Y. Liu, H.-J. Werner and J. Kästner, *J. Phys. Chem. B*, 2012, **116**, 13682–9.
- 38 T. Lin and R. Gomer, *Surf. Sci.*, 1991, **255**, 41–60.
- 39 W. Wang and Y. Zhao, *J. Chem. Phys.*, 2009, **130**, 114708.
- 40 X. D. Zhu, A. Lee, A. Wong and U. Linke, *Phys. Rev. Lett.*, 1992, **68**, 1862–1866.
- 41 Y. Suleimanov, *J. Phys. Chem. C*, 2012, **116**, 11141–11153.
- 42 E. Wigner, *Trans. Faraday Soc.*, 1938, **34**, 29.
- 43 T. J. H. Hele and S. C. Althorpe, *J. Chem. Phys.*, 2013, **138**, 084108.
- 44 T. J. H. Hele and S. C. Althorpe, *J. Chem. Phys.*, 2013, **139**, 084116.
- 45 S. C. Althorpe and T. J. H. Hele, *J. Chem. Phys.*, 2013, **139**, 084115.
- 46 D. Chandler and P. G. Wolynes, *J. Chem. Phys.*, 1981, **74**, 4078.
- 47 M. Parrinello and A. Rahman, *J. Chem. Phys.*, 1984, **80**, 860.
- 48 I. R. Craig and D. E. Manolopoulos, *J. Chem. Phys.*, 2004, **121**, 3368–3373.
- 49 S. Habershon, D. E. Manolopoulos, T. E. Markland and T. F. Miller III, *Annu. Rev. Phys. Chem.*, 2013, **64**, 387–413.
- 50 M. E. Tuckerman, *Path Integration via Molecular Dynamics*, John von Neumann Institute for Computing, NIC series, Jülich, 2002, vol. 10, pp. 269–298.
- 51 A. I. Boothroyd, W. J. Keogh, P. G. Martin and M. R. Peterson, *J. Chem. Phys.*, 1996, **104**, 7139.
- 52 J. Espinosa-García, *J. Chem. Phys.*, 2002, **116**, 10664.
- 53 Y. V. Suleimanov, R. P. de Tudela, P. G. Jambrina, J. F. Castillo, V. Sáez-Rábanos, D. E. Manolopoulos and F. J. Aoiz, *Phys. Chem. Chem. Phys.*, 2013, **15**, 3655–65.
- 54 J. W. Sutherland, M.-C. Su and J. V. Michael, *Int. J. Chem. Kinet.*, 2001, **33**, 669.
- 55 W. R. Schulz and D. J. Le Roy, *J. Chem. Phys.*, 1965, **42**, 3869.
- 56 S. L. Mielke, K. A. Peterson, D. W. Schwenke, B. C. Garrett, D. G. Truhlar, J. V. Michael, M.-C. Su and J. W. Sutherland, *Phys. Rev. Lett.*, 2003, **91**, 063201.